CCR7 ligands stimulate the intranodal motility of T lymphocytes in vivo

Tim Worbs,[1] Thorsten R. Mempel,[2] Jasmin Bölter,[1]
Ulrich H. von Andrian,[2] and Reinhold Förster[1]

[1]Institute of Immunology, Hannover Medical School, 30625 Hannover, Germany
[2]Department of Pathology, The CBR Institute for Biomedical Research, Harvard Medical School, Boston, MA 02115

In contrast to lymphocyte homing, little is known about molecular cues controlling the motility of lymphocytes within lymphoid organs. Applying intravital two-photon microscopy, we demonstrate that chemokine receptor CCR7 signaling enhances the intranodal motility of CD4$^+$ T cells. Compared to wild-type (WT) cells, the average velocity and mean motility coefficient of adoptively transferred CCR7-deficient CD4$^+$ T lymphocytes in T cell areas of WT recipients were reduced by 33 and 55%, respectively. Both parameters were comparably reduced for WT T lymphocytes migrating in T cell areas of *plt/plt* mice lacking CCR7 ligands. Importantly, systemic application of the CCR7 ligand CCL21 was sufficient to rescue the motility of WT T lymphocytes inside T cell areas of *plt/plt* recipients. Comparing the movement behavior of T cells in subcapsular areas that are devoid of detectable amounts of CCR7 ligands even in WT mice, we failed to reveal any differences between WT and *plt/plt* recipients. Furthermore, in both WT and *plt/plt* recipients, highly motile T cells rapidly accumulated in the subcapsular region after subcutaneous injection of the CCR7 ligand CCL19. Collectively, these data identify CCR7 and its ligands as important chemokinetic factors stimulating the basal motility of CD4$^+$ T cells inside lymph nodes in vivo.

CORRESPONDENCE
Reinhold Förster:
Foerster.Reinhold@
mh-hannover.de

Naive T cells constantly recirculate through LNs in search of cognate antigen (1). Upon encountering antigen in the context of peptide–MHC complexes on the surface of antigen-presenting cells, naive T cells become activated, change their movement behavior, and start to undergo rapid cell division that leads to clonal expansion of T cells specific for the antigen recognized (2–4). In an antigen-inexperienced host, the frequency of naive T cells specific for any single given antigen is extremely low, typically 1 in 10^5–10^6 T cells (5). Therefore, to allow for an effective induction of a primary immune response, it is of utmost importance that naive T cells are able to scan large areas within LNs to encounter those DCs that actually present their cognate antigen.

Several two-photon microscopy studies analyzing intranodal T cell migration in situ or after LN explantation (3, 6–8) have established a model of naive T cells migrating in a mode of random walk while scanning the T cell area. However, it remains largely unknown which factors actually determine the intranodal motility of naive T cells. Different chemokines, most prominently CCL19 and CCL21, are constitutively present in the T cell area with corresponding chemokine receptors expressed on naive T lymphocytes (9, 10). Therefore, it seems possible that chemokines act as modulators of the basal motility level of naive T cells. The key functions of CCR7 for the homing of B and T lymphocytes (10, 11) and DCs (12) to LNs, the positioning of activated B and T cells within LNs (13, 14), and the chemotaxis of activated B cells (15) and thymocytes (16) are well established. Furthermore, recent studies have suggested a chemokinetic effect of CCR7 ligands on naive T cells in vitro (17, 18); however, it is still unclear whether CCR7 signaling affects the intranodal motility of naive T lymphocytes in vivo.

In this study, we provide a detailed analysis of the role of CCR7 signaling for the motility of CD4$^+$ T cells inside the popliteal LNs (pLNs) of living animals by intravital two-photon laser-scanning microscopy. We identify CCR7 and its ligands as important chemokinetic factors stimulating the basal motility of naive CD4$^+$ T cells inside the T cell area, potentially contributing to the effective scanning of resident DCs for cognate antigen.

The online version of this article contains supplemental material.

The Journal of Experimental Medicine

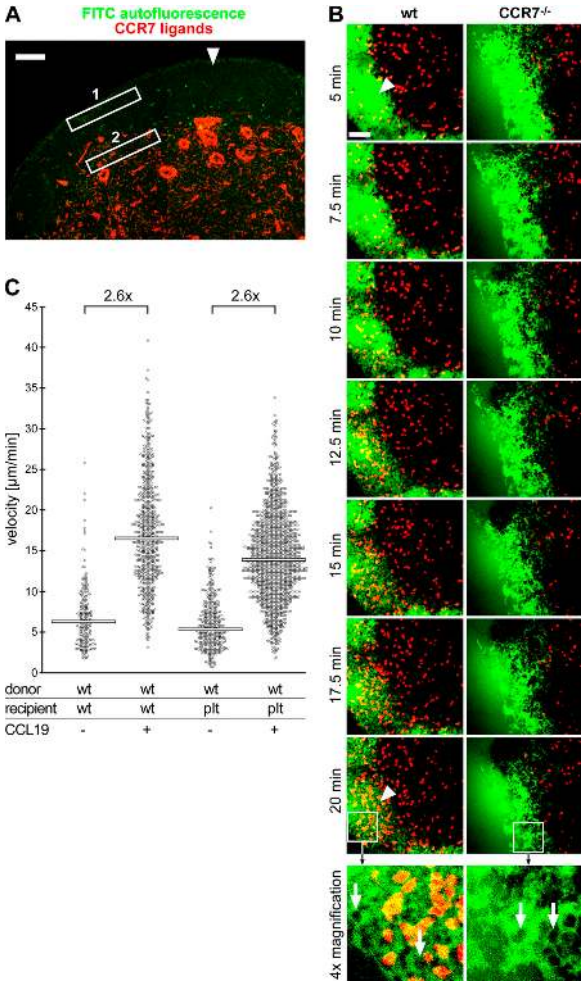

Figure 1. Analysis of CD4+ T cell motility in the subcapsular region of the pLNs before and after injection of CCL19 into the footpad. (A) Cryosection of a WT pLN stained for CCL19 plus CCL21 (red). FITC channel tissue autofluorescence (green) illustrates the outline of the LN capsule. Note the absence of CCR7 ligands in the subcapsular region (white arrow head). White frames indicate the positions of typical imaging volumes (270 × 270 × 40 µm) for the SCS region (frame 1; 20–60 µm below capsule) and T cell area (frame 2; 140–180 µm below capsule). Bar, 100 µm. (B) TAMRA-labeled WT or CCR7-deficient (CCR7$^{-/-}$) CD4$^+$ T cells were adoptively transferred into WT recipients. The subcapsular region of the pLN was imaged by intravital microscopy after injection of 1 µg CCL19 into the footpad together with FITC-labeled dextran as a tracer to highlight the SCS (green area). Screenshots of two representative movies are shown (see also Videos S1 and S3). Bar, 50 µm. Within 20 min after injection of CCL19, large numbers of highly motile TAMRA-labeled WT CD4$^+$ T cells accumulate in the SCS (white arrow heads; Video S1). In contrast, TAMRA-labeled CCR7$^{-/-}$ CD4$^+$ T cells do not migrate toward high concentrations of exogenous CCL19 (Video S3). Note that in both cases numerous nonlabeled WT host cells, visible as black "shadows" in the surrounding FITC-labeled dextran, migrate into the SCS (white arrows in 4× magnification; Video S1 and S3). (C) TAMRA-labeled WT CD4$^+$ T cells were adoptively transferred into WT or *plt/plt* (plt) recipients and the subcapsular region of the pLN was imaged by intravital microscopy before (−) or after (+) injection of 1 µg CCL19 into the footpad. Circles represent average cell velocities of individual cells, and white bars indicate median values. Graphs summarize collective data of all experiments performed (at least three independent experiments for each setup). After injection of CCL19, the median of average cell velocities of WT CD4$^+$ T cells is equally increased by a factor of 2.6 in WT and plt recipients.

RESULTS AND DISCUSSION

To directly address whether CCR7 signaling affects the intranodal motility of naive T lymphocytes, we used intravital two-photon laser-scanning microscopy of the pLNs of anesthetized mice as described previously (3), imaging the movement of CD4$^+$ T cells in different LN regions. Between 24 and 48 h after adoptive i.v. transfer of TAMRA-labeled WT CD4$^+$ T cells, WT recipients were anesthetized and the pLN was micro-surgically prepared for intravital imaging. Only very few transferred T cells were present in the subcapsular region of the LN, displaying a considerably lower average velocity (6.4 µm/min; Fig. 1 C, leftmost panel) than described for T cells in the paracortical T cell zone (10–15 µm/min) (4, 6, 15, 19, 20). This is reminiscent of earlier reports by Huang et al. (21) suggesting a correlation between T cell motility and distance to the LN surface. As shown in Fig. 1 A, CCR7 ligands are abundantly present in the paracortical T cell area but completely absent in the subcapsular region of WT LNs, fostering the idea that absence of CCR7 ligands might cause a lower overall T cell motility. To test this hypothesis, we artificially altered the regular distribution of CCR7 ligands within the pLNs by s.c. injection of 1 µg CCL19 together with FITC-labeled dextran of 150 kD as a tracer into the right hind footpad. Approximately 5 min after injection, the first TAMRA-labeled WT T cells were visibly migrating inside the subcapsular sinus (SCS), and within the next 15 min, this sinus was filled with highly motile TAMRA-labeled T cells (Fig. 1 B and Video S1, which is available at http://www.jem.org/cgi/content/full/jem.20061706/DC1). In addition to the adoptively transferred T cells, numerous nonlabeled host cells, visible as black "shadows" inside the green field of fluorescence elicited by the FITC-dextran, migrated inside the SCS. We could not identify the exact "route of entry" of these cells in our imaging setup; however, we can exclude a recruitment into the SCS via afferent lymphatics (Video S2). We therefore speculate that under the chemotactic influence of high CCL19 concentrations inside the SCS, WT cells are possibly recruited into the SCS via the medullary sinus by retrograde migration. When, on the other hand, CCR7$^{-/-}$ CD4$^+$ T cells had been transferred into WT recipients, the s.c. injection of CCL19 failed to induce mobilization of TAMRA-labeled CCR7$^{-/-}$ cells into the SCS, whereas unlabeled endogenous WT cells were amply present in this area (Fig. 1 B and Video S3).

To quantitatively characterize this CCR7-mediated cell motility in the SCS, we imaged different parts of the subcapsular region of the pLN at depths of ~20–60 µm in WT as well as in *plt/plt* (plt) recipients, with the latter completely lacking intranodal CCR7 ligands. Although the few WT CD4$^+$ T cells present under physiological conditions in the subcapsular area of the pLN exhibited equally low average velocities in both recipients (WT, 6.4 µm/min; plt, 5.4 µm/min;

Fig. 1 C), we observed a dramatic increase in the motility of WT donor T cells in the SCS region in the presence of exogenous CCL19. Importantly, this holds true for WT as well as for plt recipients, as the median of the average cell velocities equally increased by a factor of 2.6 (from 6.4 to 16.6 μm/min in WT, and from 5.4 to 14.0 μm/min in plt recipients; Fig. 1 C). These results demonstrate that the basic migration behavior of adoptively transferred WT T cells is comparable in superficial LN areas of WT and plt recipients and seems to be influenced by the presence or absence of CCR7 ligands in a given region of the organ.

To further elucidate the importance of CCR7 signaling for the intranodal motility of $CD4^+$ T cells, we subsequently analyzed the LN compartment in which CCR7 ligands are naturally present (Fig. 1 A). We therefore imaged adoptively transferred WT or $CCR7^{-/-}$ $CD4^+$ T cells in the paracortical T cell areas of WT and plt recipients at imaging depths of 120–200 μm below the LN capsule. At first glance, the overall mode of movement seemed to be comparable in the presence or absence of CCR7 signaling (Fig. 2 A). However, the velocity was obviously reduced for $CCR7^{-/-}$ T cells in WT recipients and for WT T cells migrating in the T cell zone of

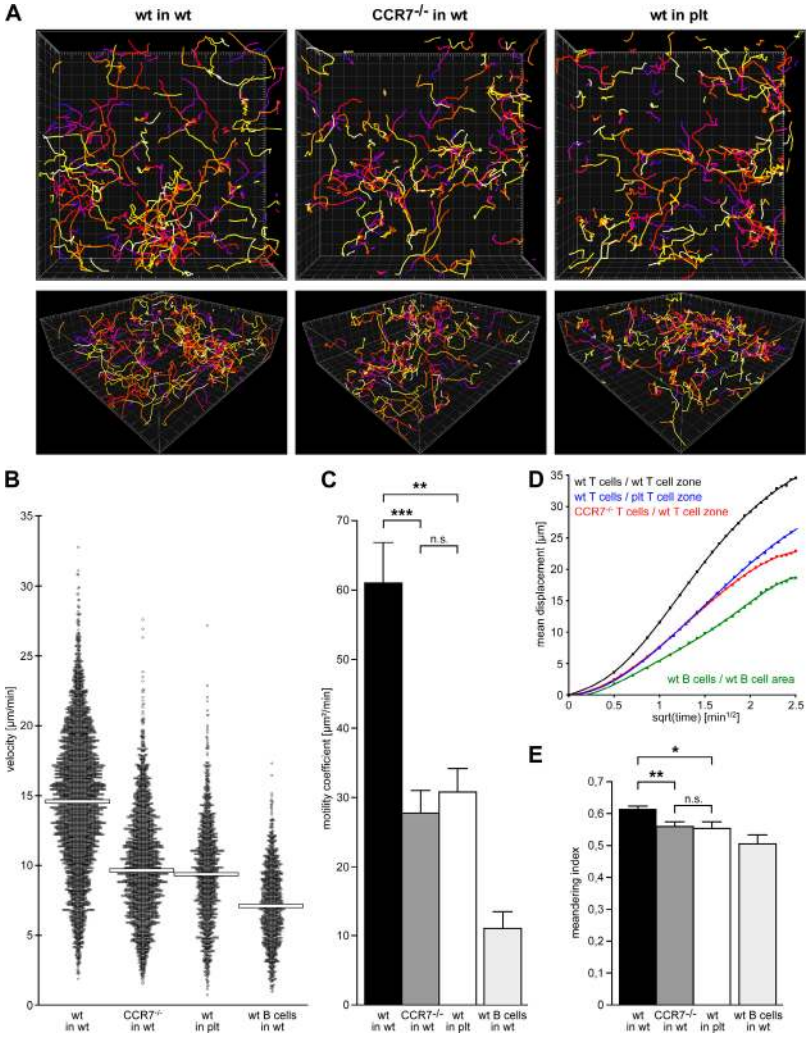

Figure 2. Quantitative analysis of $CD4^+$ T lymphocyte movement behavior in the T cell zone. TAMRA-labeled WT or CCR7-deficient ($CCR7^{-/-}$) $CD4^+$ T cells were adoptively transferred into WT or *plt/plt* (plt) recipients, and the T cell area of the pLN was imaged by intravital microscopy. (A) Automated tracking of $CD4^+$ T lymphocyte migration in the T cell zone. 150 randomly chosen trajectories of individual cells are displayed as color-coded tracks to represent increasing time from blue (start of imaging) to yellow (end of imaging). A representative imaging session of 15 min is shown for each experimental setting (see also Videos S4–S6). In the bottom panel, images are rotated to display the z dimension of the imaged volumes. Grid spacing (distance between major tick marks) is 10 μm for x, y, and z orientation in all images. (B) Average cell velocity. Circles represent average cell velocities of individual cells, and white bars indicate median values. (C) MC (mean ± SEM). (D) Mean displacement plot. The approximately linear curves indicate random walk movement in all experimental settings analyzed. (E) Meandering index (mean ± SEM). Motility parameters of WT B cells imaged in B cell follicles of WT recipients (WT B cells in WT) are shown for comparison. Graphs summarize collective data of all experiments (at least three independent experiments for each setup). *, $P \leq 0.1$; **, $P \leq 0.05$; ***, $P \leq 0.01$. n.s., not significant.

plt recipients (Videos S4–S6, available at http://www.jem.org/cgi/content/full/jem.20061706/DC1). The quantitative analysis by automated cell tracking confirmed these observations, revealing a significant decrease of the median of the average cell velocities of CCR7$^{-/-}$ T cells (WT, 14.6 μm/min vs. CCR7$^{-/-}$, 9.7 μm/min; Fig. 2 B). Of interest, WT CD4$^+$ T cells in the paracortical T cell areas of plt recipients showed a comparably reduced motility (median of average cell velocities, 9.4 μm/min; Fig. 2 B). This indicates that CCR7 signaling indeed affects the basal velocity level of T lymphocytes inside the T cell area of noninflamed LNs.

Analogous to Miller et al. (19) we calculated the mean motility coefficient (MC), representing the propensity of a cell to move away from its original starting position. This general motility parameter is largely reduced once CCR7 or its ligands are missing (WT T cells in WT recipient, 61.0 ± 5.8 μm^2/min; CCR7$^{-/-}$ T cells in WT recipient, 27.7 ± 3.3 μm^2/min; WT T cells in plt recipient, 30.7 ± 3.5 μm^2/min; for comparison, WT B cells in WT recipient, 11.1 ± 2.5 μm^2/min; Fig. 2 C). These findings strongly indicate that the reduced intranodal velocity of T lymphocytes in the absence of CCR7 signaling is associated with a reduced ability to effectively sweep large parts of the T cell area that could lead to T cells contacting fewer DCs per time in their search for cognate antigen.

Plotting the mean displacement of all tracked cells for any given experimental condition over the square root of time yields in all cases a pattern that is in accordance with random walk movements (Fig. 2 D). Therefore, lack of CCR7 signaling obviously does not alter the general mode of T cell movement. The meandering index (total displacement/path length of a cell track) allows for a more detailed analysis of the straightness of T lymphocyte movement, with a value of 1 representing a completely linear cell track. As displayed in Fig. 2 E, there was only a minor reduction of the mean meandering index in the absence of CCR7 signaling (WT T cells in WT recipient, 0.61 ± 0.01; CCR7$^{-/-}$ T cells in WT recipient, 0.56 ± 0.02; WT T cells in plt recipient, 0.55 ± 0.02; for comparison, WT B cells in WT recipient, 0.50 ± 0.03). Analysis of the turning angle distribution confirms this result, as CD4$^+$ T cells in the absence of CCR7 signaling turn at slightly larger turning angles, indicating sharper turns and therefore a less linear movement (not depicted).

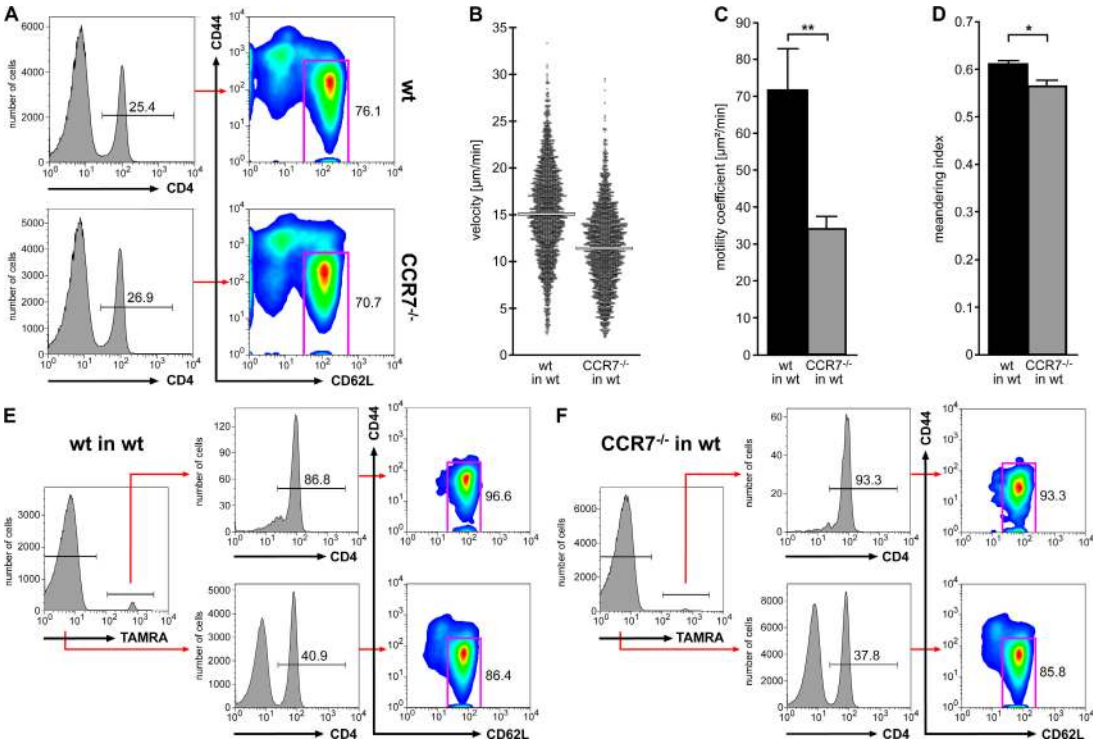

Figure 3. Motility analysis of naive CD4$^+$ T lymphocytes in the T cell zone of WT recipients. (A) FACS analysis of lymphocyte subsets before cell sorting. Comparable proportions of naive (CD62L$^+$CD44^{low}) CD4$^+$ T cells are present in pooled peripheral LNs and spleens from WT (WT) and CCR7$^{-/-}$ (CCR7$^{-/-}$) donor mice. After FACS sorting for CD4$^+$CD44^{low}, TAMRA-labeled WT or CCR7-deficient (CCR7$^{-/-}$) naive T cells were adoptively transferred into WT recipients, and the T cell area of the pLN was imaged by intravital microscopy. Graphs summarize collective data of all experiments (two independent experiments for each setup). (B) Average cell velocity. Circles represent average cell velocities of individual cells, and white bars indicate median values. (C) MC (mean ± SEM). (D) Meandering index (mean ± SEM). *, P ≤ 0.1; **, P ≤ 0.05. (E and F) FACS analysis of adoptively transferred TAMRA$^+$ WT (E) and CCR7$^{-/-}$ (F) lymphocytes isolated from peripheral LNs of WT recipient mice after completion of intravital imaging. In both cases, the TAMRA$^+$ population contains mostly naive (CD62L$^+$CD44^{low}) CD4$^+$ T cells. Numbers indicate percentage of gated cells. Data shown are representative for two experiments.

Analyzing lymphocytes isolated from pooled LNs and spleens of WT and CCR7$^{-/-}$ animals, we found comparable percentages of naive (CD62L^{+} CD44^{low}) cells within the CD4^{+} T cell population (WT, 76.1%; CCR7$^{-/-}$, 70.7%; Fig. 3 A). However, transfer of MACS-purified bulk CD4^{+} T cells might nonetheless have introduced a selectional bias in the motility analysis because nonnaive T cell subsets, potentially exhibiting a different intrinsic motility, could have been preferentially recruited to LNs in the absence of CCR7 function. We therefore repeated these experiments with WT and CCR7$^{-/-}$ CD4^{+} T cells that were additionally sorted for low expression of CD44 before adoptive transfer. In both cases, the total percentage of CD4^{+} CD44^{low} T cells was equally increased from ~19 to ~84% by FACS sorting (not depicted). Imaging the motility of the transferred naive CD4^{+} CD44^{low} T lymphocytes in the T cell area of WT recipients, we obtained results comparable to the experiments using bulk CD4^{+} T cells. The median of the average cell velocities was slightly increased for both WT and CCR7$^{-/-}$ cells (WT, 15.1 μm/min vs. CCR7$^{-/-}$, 11.4 μm/min; Fig. 3 B). The same holds true for the MC (WT T cells in WT recipient, 71.8 ± 11.2 μm^2/min; CCR7$^{-/-}$ T cells in WT recipient, 34.1 ± 3.3 μm^2/min; Fig. 3 C), whereas the mean meandering indices were almost unchanged (WT T cells in WT recipient, 0.61 ± 0.01; CCR7$^{-/-}$ T cells in WT recipient, 0.56 ± 0.01; Fig. 3 D). After completion of intravital microscopy, the recipient mice were analyzed by FACS for the subset composition of TAMRA-labeled cells that had homed into peripheral LNs (and were therefore subject to the imaging analysis). As depicted in Fig. 3 (E and F), TAMRA^{+} cells found in peripheral LNs were mostly naive (CD62L^{+} CD44^{low}) CD4^{+} T cells after transfer of WT (96.6% of transferred CD4^{+} T cells) as well as of CCR7$^{-/-}$ (93.3% of transferred CD4^{+} T cells) cells, ruling out an influence of biased homing of different T cell subsets on the motility analysis performed in these experiments (for a direct comparison of CD44 expression levels see Fig. S1, available at http://www.jem.org/cgi/content/full/jem.20061706/DC1). Collectively, these results demonstrate that CCR7 and its ligands positively influence the intranodal cell migration speed of naive CD4^{+} T lymphocytes, whereas the directionality of T cell movement behavior is largely unaffected by lack of CCR7 function.

Finally, we aimed to directly visualize the alteration of intranodal T cell motility by manipulation of CCR7 signaling during imaging (Fig. 4). 24 h after adoptive transfer of CD4^{+} WT T cells into plt recipients, mice were i.v. injected with 200 μg anti-CD62L mAb to block any further homing of lymphocytes to LNs (3). Imaging the movement behavior of T lymphocytes in the paracortical T cell zone 2 h later, we observed a significant reduction of T cell velocity and MC compared with the movement of WT T cells in WT recipients (Fig. 4, A and B; see also Fig. 2). To restore the presence of CCR7 ligands within the LNs of the plt recipients, we subsequently i.v. injected 100 μg CCL21. During the next 2.5 h of imaging, the motility of WT T cells in the plt T cell area increased substantially. Within this time period, velocity and MC reached approximately levels observed imaging WT T cells in WT recipients (Fig. 4, A and B; see also Fig. 2), whereas the meandering index was only moderately increased (Fig. 4 C). This reversal of the motility reduction observed in the absence of CCR7 ligands (T cell zone of untreated plt recipients) by systemic application of CCL21 strongly argues for a direct positive influence of CCR7 signaling on the intranodal motility of T lymphocytes.

The velocities of WT T cells reported in this study are in good agreement with data of existing two-photon microscopy studies of in situ and explanted LNs. Zinselmeyer et al. (20) also reported 15 μm/min for CD4^{+} T cells in explanted LNs, and Okada et al. (15) found ~14 μm/min for helper T cells in a similar setup. Earlier studies by Miller et al. (4, 6, 19) resulted in somewhat lower T cell velocities of 10–12 μm/min. Importantly, Miller et al. performed the cell tracking on z-projections of the imaging volumes, thereby obtaining lateral velocities for movements in the xy-plane only. This should result in velocity values that are by a factor of square root (3/2) = 1.225 lower compared with three-dimensional cell tracking, as the z-compound of the movement vector is not contributing to the velocity calculation (assuming that a T lymphocyte migrating in the T cell area of a LN by random walk does not exhibit any directional bias). The velocity of WT B cells (7.1 μm/min) is also comparable to previously published data (15, 19), further confirming the validity of the experimental setup used.

Previous in vitro studies suggested that the higher motility of T cells migrating in a three-dimensional collagen gel in the presence of DCs could be due to soluble factors secreted by

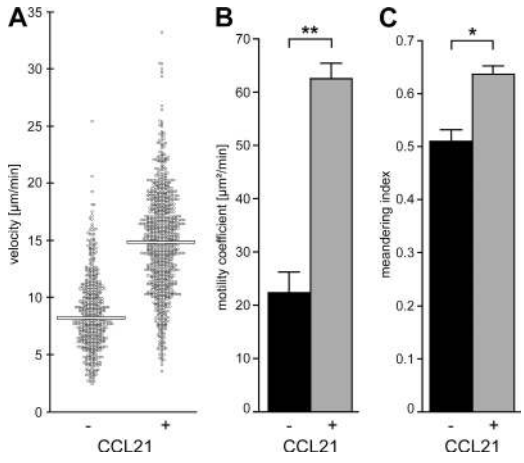

Figure 4. Systemic CCL21 application restores the motility of WT CD4^{+} T lymphocytes in the T cell area of plt recipients. TAMRA-labeled WT CD4^{+} T cells were adoptively transferred into plt recipients, and the T cell area of the pLN was imaged by intravital microscopy before (−) and 2.5 h after (+) i.v. injection of 100 μg CCL21. Graphs summarize collective data of all experiments (two independent experiments). (A) Average cell velocity. Circles represent average cell velocities of individual cells, and white bars indicate median values. (B) MC (mean ± SEM). (C) Meandering index (mean ± SEM). *, $P \leq 0.1$; **, $P \leq 0.05$.

DCs (22), and that CCL19 might have a positive effect on the scanning behavior of naive T cells (17). During the submission process of this article, Stachowiak et al. (18) reported that CCL19 and CCL21 induce long-lived chemokinesis in $CD4^+$ T cells migrating on different adhesion molecules in vitro, further supporting the in vivo analysis of the present study.

Using intravital microscopy, we provide for the first time direct in vivo evidence for a chemokinetic function of CCR7 and its ligands stimulating the intranodal basal motility of naive T lymphocytes. Interestingly, a recent study by Bajenoff et al. (23) provides evidence that the fibroblastic reticular cell network essentially defines and supports the apparent random walk movement of naive T cells within the LN paracortex. It therefore seems possible that CCR7 ligands immobilized on fibroblastic reticular cells or extracellular matrix surfaces, rather than soluble chemokines, are mediating the observed CCR7-dependent stimulation of the intranodal T cell velocity. Regardless of the actual state of the chemokines involved, the enhanced motility allows for a faster, more widespread movement of T cells in the T cell area, thereby potentially enhancing the likelihood of encounters with resident DCs presenting rare cognate antigens. In light of these findings, it seems possible that a reduced scanning performance, in addition to the known homing defects, could contribute to the delayed and in some cases impaired immune responses observed in $CCR7^{-/-}$ animals. It will be interesting to see in subsequent studies how other parameters, such as recruitment of inflammatory cells or ongoing immune responses, influence intranodal T cell motility.

MATERIALS AND METHODS

Animals. C57BL/6, C57BL/6 $CCR7^{-/-}$, and C57BL/6 *plt/plt* were bred at the animal facility of Hannover Medical School under specific pathogen-free conditions. Animal experiments have been approved by the institutional review board and local authorities.

Antibodies and reagents. Anti-CD3 (clone 17A2), anti-CD4 (clone RMCD4), anti-CD62L (clone MEL-14), and anti-B220 (clone TIB 146) antibodies were provided by E. Kremmer (GSF, Munich, Germany) and used in the following conjugations: anti–CD3-Cy5, anti–CD4-Pacific-Orange, anti–CD4-Cy5, and anti–B220-Cy5. These antibodies were also used in this study: anti–CD44-APC, anti–CD62L-FITC, StreptAvidin–PE-Cy7 (BD Biosciences), goat anti-mCCL19, goat anti-mCCL21 (R&D Systems), donkey anti–goat IgG-peroxidase (Jackson ImmunoResearch Laboratories). 150 kD of FITC-labeled dextran was obtained from Sigma-Aldrich, and recombinant mCCL19 was from R&D Systems.

Immunohistology. Acetone-fixed 8-μm cryosections of pLNs were rehydrated, preincubated with 10% mouse serum, and stained with a cocktail of antibodies in 2.5% serum. Nuclei were stained with DAPI. Images were acquired using a Zeiss Axiovert 200 M microscope. Detection of anti-mCCL19/anti-mCCL21 antibody binding was enhanced using the TSA-Cy3 Tyramid Signal Amplification system (PerkinElmer).

Adoptive transfers. 6–8-wk-old donor mice (C57BL/6 or C57BL/6 $CCR7^{-/-}$) were killed by CO_2 inhalation, and single cell suspensions were prepared from spleens and LNs (mesenteric, inguinal, brachial, and axillary). After erylysis, cells were labeled with 10 μM 5-(and-6-)-TAMRA SE or 5 μM CFSE (Invitrogen) for 15 min at 37°C. Untouched $CD4^+$ T lymphocytes were isolated using a MACS $CD4^+$ T cell isolation kit together with an AutoMACS (Miltenyi Biotec). Alternatively, cells were stained with the biotin antibody cocktail followed by StreptAvidin–PE-Cy7 and anti–CD44-APC, and cell sorting for PE-$Cy7^-$/$CD44^{low}$ cells was performed on a FACSAria (BD Biosciences). $B220^+$ B cells were purified using anti-B220 MACS microbeads. The purity of cell preparations after MACS was always >90%. 6–8-wk-old WT or plt recipients received 1–1.25 × 10^7 WT $CD4^+$ T or $B220^+$ B cells or 1.5–2.5 × 10^7 $CCR7^{-/-}$ $CD4^+$ T cells by i.v. injection. Dye labeling (CFSE or TAMRA) was swapped between experiments. In most experiments, only TAMRA-labeled cells were used.

Intravital microscopy. Between 24 and 48 h after adoptive transfer, mice were anaesthetized by an initial i.p. injection of 100 mg/kg ketamine and 1 mg/kg medetomidine. In some experiments, mice received a single i.v. injection of 200 μg anti-CD62L mAb (clone MEL-14) 2 h before imaging commenced to prevent further homing of lymphocytes to LNs. The animal was placed on a custom-built preparation stage fixating the right hind leg. The right pLN was micro-surgically prepared free of overlying connective and adipose tissue, submerged in normal saline and covered with a glass coverslip. Special care was taken to spare blood vessels and afferent lymphatic vessels during microsurgery. A thermocouple was placed next to the LN to monitor local temperature, which was maintained at 36.5 ± 1°C. Two-photon laser scanning microscopy was performed with an upright Leica DM LFSA microscope equipped with a 20× 0.95 NA water immersion objective (Olympus) and a MaiTai Ti:sapphire-pulsed laser (Spectra-Physics). For two-photon excitation, the MaiTai laser was tuned to 858 nm. Green (CFSE or FITC) and red (TAMRA) fluorescence emission was detected with nondescanned detectors fitted with 535/50 and 610/75 band path filters, respectively. To generate time-lapse series, stacks of 10–11 x-y sections with 4–4.5-μm spacing were acquired every 15 or 20 s with 1.5–2.5× electronic zoom providing imaging volumes 40–50 μm in depth and 215–360 μm in width. Exogenous chemokine (1 μg of recombinant mCCL19 in 30 μl of normal saline containing 5 μg of FITC-labeled dextran of 150 kD as tracer) was injected s.c. into the right hind footpad.

Data analysis. Imaris (Bitplane) was used for four-dimensional image analysis and automated tracking of cells. The accuracy of the automated tracking was manually controlled, and only tracks with durations of >60 s were included in the analysis. Average cell velocity and meandering index were calculated using Imaris, and turning angle distribution, mean displacement, and MC were calculated using SciLab after exporting the x, y, and z coordinates of spot positions. Statistical analysis was performed with GraphPad Prism 4. Results are displayed as individual data points plus median or mean ± SEM summarizing collective data from all experiments performed. All significant values were determined using the unpaired two-tailed *t* test.

Online supplemental material. Video S1 shows the accumulation of highly motile transferred TAMRA-labeled WT $CD4^+$ T cells as well as of unlabeled endogenous WT T cells in the SCS of the pLNs after s.c. injection of exogenous CCL19 into the hind footpad. As exemplified by Video S2, there is no evidence for immigration of T cells into the SCS via the afferent lymphyatics after injection of exogenous CCL19. Video S3 shows the absence of TAMRA-labeled $CCR7^{-/-}$ $CD4^+$ T cells inside the SCS in the same experimental setting, whereas unlabeled endogenous cells of the WT recipient exhibit a strong migratory response. Videos S4–S6 illustrate the motility of transferred TAMRA-labeled T cells within the T cell zone of the pLNs (Video S4, WT T cells in WT recipient; Video S5, $CCR7^{-/-}$ T cells in WT recipient; Video S6, WT T cells in plt recipient). As depicted in Fig. S1, no enrichment of nonnaive $CD44^{high}$ lymphocytes was observed after adoptive transfer of $CD4^+$ T cells in the absence of CCR7 signaling. The online supplemental material is available at http://www.jem.org/cgi/content/full/jem.20061706/DC1.

We are especially grateful to Stefanie Willenzon for excellent technical assistance and Oliver Pabst and Günter Bernhardt for discussion and critical comments on the manuscript.

This study has been supported by DFG grants SFB566-A14 and SFB587-B3 to R. Förster.

The authors have no conflicting financial interests.

Submitted: 9 August 2006
Accepted: 26 January 2007

REFERENCES

1. Gowans, J.L., and E.J. Knight. 1964. The route of re-circulation of lymphocytes in the rat. *Proc. R. Soc. Lond. B. Biol. Sci.* 159:257–282.
2. Banchereau, J., and R.M. Steinman. 1998. Dendritic cells and the control of immunity. *Nature.* 392:245–252.
3. Mempel, T.R., S.E. Henrickson, and U.H. Von Andrian. 2004. T-cell priming by dendritic cells in lymph nodes occurs in three distinct phases. *Nature.* 427:154–159.
4. Miller, M.J., O. Safrina, I. Parker, and M.D. Cahalan. 2004. Imaging the single cell dynamics of CD4$^+$ T cell activation by dendritic cells in lymph nodes. *J. Exp. Med.* 200:847–856.
5. von Andrian, U.H., and C.R. Mackay. 2000. T-cell function and migration. Two sides of the same coin. *N. Engl. J. Med.* 343:1020–1034.
6. Miller, M.J., S.H. Wei, M.D. Cahalan, and I. Parker. 2003. Autonomous T cell trafficking examined in vivo with intravital two-photon microscopy. *Proc. Natl. Acad. Sci. USA.* 100:2604–2609.
7. Bousso, P., and E. Robey. 2003. Dynamics of CD8+ T cell priming by dendritic cells in intact lymph nodes. *Nat. Immunol.* 4:579–585.
8. Miller, M.J., A.S. Hejazi, S.H. Wei, M.D. Cahalan, and I. Parker. 2004. T cell repertoire scanning is promoted by dynamic dendritic cell behavior and random T cell motility in the lymph node. *Proc. Natl. Acad. Sci. USA.* 101:998–1003.
9. Luther, S.A., H.L. Tang, P.L. Hyman, A.G. Farr, and J.G. Cyster. 2000. Coexpression of the chemokines ELC and SLC by T zone stromal cells and deletion of the ELC gene in the plt/plt mouse. *Proc. Natl. Acad. Sci. USA.* 97:12694–12699.
10. Forster, R., A. Schubel, D. Breitfeld, E. Kremmer, I. Renner-Muller, E. Wolf, and M. Lipp. 1999. CCR7 coordinates the primary immune response by establishing functional microenvironments in secondary lymphoid organs. *Cell.* 99:23–33.
11. Stein, J.V., A. Rot, Y. Luo, M. Narasimhaswamy, H. Nakano, M.D. Gunn, A. Matsuzawa, E.J. Quackenbush, M.E. Dorf, and U.H. von Andrian. 2000. The CC chemokine thymus-derived chemotactic agent 4 (TCA-4, secondary lymphoid tissue chemokine, 6Ckine, exodus-2) triggers lymphocyte function–associated antigen 1–mediated arrest of rolling T lymphocytes in peripheral lymph node high endothelial venules. *J. Exp. Med.* 191:61–76.
12. Ohl, L., M. Mohaupt, N. Czeloth, G. Hintzen, Z. Kiafard, J. Zwirner, T. Blankenstein, G. Henning, and R. Forster. 2004. CCR7 governs skin dendritic cell migration under inflammatory and steady-state conditions. *Immunity.* 21:279–288.
13. Reif, K., E.H. Ekland, L. Ohl, H. Nakano, M. Lipp, R. Forster, and J.G. Cyster. 2002. Balanced responsiveness to chemoattractants from adjacent zones determines B-cell position. *Nature.* 416:94–99.
14. Hardtke, S., L. Ohl, and R. Forster. 2005. Balanced expression of CXCR5 and CCR7 on follicular T helper cells determines their transient positioning to lymph node follicles and is essential for efficient B-cell help. *Blood.* 106:1924–1931.
15. Okada, T., M.J. Miller, I. Parker, M.F. Krummel, M. Neighbors, S.B. Hartley, A. O'Garra, M.D. Cahalan, and J.G. Cyster. 2005. Antigen-engaged B cells undergo chemotaxis toward the T zone and form motile conjugates with helper T cells. *PLoS Biol.* 3:e150.
16. Witt, C.M., S. Raychaudhuri, B. Schaefer, A.K. Chakraborty, and E.A. Robey. 2005. Directed migration of positively selected thymocytes visualized in real time. *PLoS Biol.* 3:e160.
17. Kaiser, A., E. Donnadieu, J.P. Abastado, A. Trautmann, and A. Nardin. 2005. CC chemokine ligand 19 secreted by mature dendritic cells increases naive T cell scanning behavior and their response to rare cognate antigen. *J. Immunol.* 175:2349–2356.
18. Stachowiak, A.N., Y. Wang, Y.C. Huang, and D.J. Irvine. 2006. Homeostatic lymphoid chemokines synergize with adhesion ligands to trigger T and B lymphocyte chemokinesis. *J. Immunol.* 177:2340–2348.
19. Miller, M.J., S.H. Wei, I. Parker, and M.D. Cahalan. 2002. Two-photon imaging of lymphocyte motility and antigen response in intact lymph node. *Science.* 296:1869–1873.
20. Zinselmeyer, B.H., J. Dempster, A.M. Gurney, D. Wokosin, M. Miller, H. Ho, O.R. Millington, K.M. Smith, C.M. Rush, I. Parker, et al. 2005. In situ characterization of CD4$^+$ T cell behavior in mucosal and systemic lymphoid tissues during the induction of oral priming and tolerance. *J. Exp. Med.* 201:1815–1823.
21. Huang, A.Y., H. Qi, and R.N. Germain. 2004. Illuminating the landscape of in vivo immunity: insights from dynamic in situ imaging of secondary lymphoid tissues. *Immunity.* 21:331–339.
22. Gunzer, M., A. Schafer, S. Borgmann, S. Grabbe, K.S. Zanker, E.B. Brocker, E. Kampgen, and P. Friedl. 2000. Antigen presentation in extracellular matrix: interactions of T cells with dendritic cells are dynamic, short lived, and sequential. *Immunity.* 13:323–332.
23. Bajenoff, M., J.G. Egen, L.Y. Koo, J.P. Laugier, F. Brau, N. Glaichenhaus, and R.N. Germain. 2006. Stromal cell networks regulate lymphocyte entry, migration, and territoriality in lymph nodes. *Immunity.* 25:989–1001.